J. Fluid Mech. (2006), *vol.* 549, *pp.* 141–157.
doi:10.1017/S0022112005007561 Printed in the United Kingdom

A numerical model for withdrawal from a two-layer fluid

By D. E. FARROW AND G. C. HOCKING

Mathematics and Statistics, Division of Science and Engineering, Murdoch University, Murdoch, WA 6150, Australia

(Received 24 August 2004 and in revised form 27 July 2005)

This paper reports the results of several direct numerical simulations of the withdrawal of a two-layer fluid with a finite-thickness interface through a slot in the base of a finite rectangular cavity. Particular attention is paid to the role of long (basin scale) interfacial waves on the processes leading to drawdown of the interface into the slot. It is shown that these waves play an important role and can either delay or accelerate drawdown. This means that drawdown can occur over a range of Froude numbers. The results are compared with previous work for ideal flow and experimental results.

1. Introduction

The withdrawal of water from a fluid consisting of several layers of different density has a range of engineering applications and as a consequence it has been the subject of a considerable amount of research. It is important for achieving various quality constraints in drinking water, and in modelling physical processes to manage a reservoir better. Withdrawal and inflow to solar ponds are used to extract energy and to control the stratification in the pond in order to maintain stability and optimize efficiency. In power station cooling ponds, efficient operation can be maintained by paying careful attention to withdrawal (Imberger & Hamblin 1982).

A series of theoretical papers (for example, Landrini & Tyvand 2001; Stokes, Hocking & Forbes 2003 and references therein) has provided a detailed map of the qualitative behaviour of the interface between two layers of different densities when drawing from the lower layer, making a range of (reasonable) assumptions that make the problem solvable. The main assumptions have been that the layers are immiscible, the interface is of infinitesimal extent and that the fluid is inviscid and the flow irrotational. In addition, various assumptions have been made about the geometry of the flow domain, usually including that the withdrawal point is a line or point sink and that the fluid has at least infinite horizontal extent. These assumptions allow steady-state and, more recently, unsteady solutions for potential flows (ideal fluid) with nonlinear free-surface conditions. These have provided a strong guide to the behaviour, as outlined below.

It has long been known that the withdrawal all occurs from within the layer adjacent to the withdrawal point until some critical flow rate is reached, after which water from both layers is drawn out directly through the sink. Tyvand (1992), Landrini & Tyvand (2001) and Stokes *et al.* (2003) have shown, however, that this critical event is not as clear cut as was originally thought. In effect, there are a range of possibilities for the occurrence of the 'critical drawdown' that depend strongly on the flow history. These can be roughly classified into two groups: the first in which the dip in the

interface generated by the initiation of the sink causes immediate drawdown of the interface; and the second at a higher flow rate if the first group is avoided.

However, it is not clear how the flow is affected by each of the idealizations made in previous work. What is the effect of having an interfacial gradient? How do the waves reflected from the end of the tank affect the outcome? How small does the outlet have to be to allow its approximation by a line or point sink? In this paper, we describe a series of numerical experiments performed using a finite-difference code to incorporate all of these factors and examine how they influence the general behaviour described above.

Experiments (for example, Jirka 1979; Hocking 1991) show that the qualitative behaviour of the flow when withdrawal occurs through a narrow horizontal slot in the vertical endwall of a rectangular tank containing two homogeneous layers of different density is as follows. If the slot is situated within the lower layer, buoyancy forces ensure that only fluid from the lower layer is drawn through the slot at low flow rates. At this time, there is a very slow (compared to the flow in the lower layer) circulation of the fluid in the upper layer. The interface between the two layers remains approximately horizontal once the transient wave motion caused by opening the slot has dissipated, except for a slight thickening of the interface near the wall directly above the slot. As the depth of the lower layer decreases, the effective flow rate increases, and at some critical value, the interface is suddenly pulled down and enters the slot directly, so that the upper layer also begins to flow out through the slot. This critical transition occurs rapidly compared with the previous flow development. Once above this critical flow rate, the angle at which the interface enters the slot decreases as the effective flow rate increases. However, this experimental work has shown that there is a large scatter in the values of the critical flow rate, and a theoretical investigation of the flow is important in interpreting results obtained in experiments and in the field.

Craya (1949) approximated the subcritical flow (i.e. when only the lower layer is being withdrawn) as a steady irrotational motion of an inviscid incompressible fluid, and the withdrawal slot by a line sink. This assumption necessitates the solution of Laplace's equation in the fluid domain subject to conditions that ensure continuity of pressure across the interface and prohibit flow through the boundaries or across the interface. The problem is further complicated by the fact that the location of the interface is unknown. This model of the flow clearly neglects some features which may be of importance in determining the exact details of the flow in a real situation, such as viscous effects near the walls and along the interface, the time-dependent nature of the flow as the level falls, and the transient effects of opening the slot.

Pao & Kao (1974) derived a linear model for general stratification to determine the internal wave activity in a horizontal duct and hence investigate selective withdrawal. Kao (1976) considered the case of a two-layer stratification similar to the case here, but with a domain of infinite horizontal and vertical extent and with the sink in the middle of the interface.

For withdrawal through a slot, i.e. the two-dimensional problem, the experimental work is restricted to that of Gariel (1949), Harleman & Elder (1965); Wood & Lai (1972) and Hocking (1991). In almost all of these cases it was found that the critical drawdown point, at which the upper fluid begins to flow out through the sink, occurs at a Froude number much lower than that predicted by the theoretical solutions described above. This is consistent with the experimental results for a point sink, in which the drawdown occurs at much lower values of the Froude number than

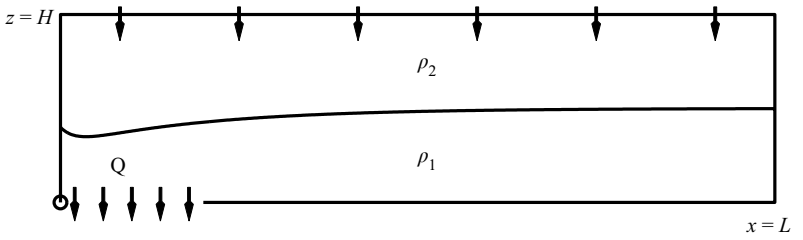

FIGURE 1. Schematic of flow domain showing coordinate system and location of the sink.

expected (Harleman & Elder 1965; Jirka & Katavola 1979; Lawrence & Imberger 1979).

In this paper, a finite-difference approach is used to simulate the withdrawal of water through a slot in the bottom from a tank containing two layers of different density separated by a reasonably thin interface. The goal is to compare the qualitative aspects of the full Navier–Stokes simulation with the ideal fluid theory used extensively to examine this problem. The model formulation is similar to that of Kao (1976) except that here the domain is finite and the sink is located in the base.

2. Model formulation

Figure 1 shows a schematic of the flow domain. For $t > 0$, fluid leaves the cavity through the base near the left-hand wall at a maximum rate $Q\,\mathrm{m}^2\,\mathrm{s}^{-1}$. The sink is placed in the base of the domain as the flow domain is thought of as a half-domain. There is a line of symmetry at $x = 0$ where horizontal gradients of all variables vanish. Fluid enters the cavity at $z = H$ at the same flow rate. The upper boundary condition is $w = -Q/L$, i.e. a uniform velocity. This mimics the laboratory situation where the air/water interface would be only slightly perturbed by the turning on of the sink and would simply 'fall' at whatever rate is required to ensure conservation of volume. It is assumed that the fluid entering the cavity has the same density as the fluid at $z = H$.

So long as density perturbations from the mean value ρ_0 are small, the Boussinesq approximation is appropriate. The system is non-dimensionalised using the length scale H, time scale H^2/Q, velocity scale Q/H and density scale $\Delta\rho_0/2$ where $\Delta\rho_0$ is the initial density difference between the two layers. The major parameters of the problem are then the bulk Froude number $Fr_0 = Q/\sqrt{g'H^3}$ where $g' = (\Delta\rho_0 g/\rho_0)/2$ is the reduced gravity, the Reynolds number $Re = Q/\nu$ and the aspect ratio of the cavity $A = H/L$. The dimensionless flow domain is $0 < x < A^{-1}$ and $0 < z < 1$. The dimensionless equations of motion are

$$\frac{\mathrm{D}u}{\mathrm{D}t} = -\frac{\partial p}{\partial x} + \frac{1}{Re}\nabla^2 u, \tag{2.1}$$

$$\frac{\mathrm{D}w}{\mathrm{D}t} = -\frac{\partial p}{\partial z} + \frac{1}{Re}\nabla^2 w - \frac{1}{Fr_0^2}\rho, \tag{2.2}$$

$$\frac{\mathrm{D}\rho}{\mathrm{D}t} = \frac{1}{\sigma Re}\nabla^2 \rho, \tag{2.3}$$

$$\frac{\partial u}{\partial z} + \frac{\partial w}{\partial z} = 0, \tag{2.4}$$

where $\sigma = \nu/\kappa$ is the Prandtl number and κ is the diffusivity of the stratifying species. The boundary conditions are

$$u_z = 0, \;\; w = -Ar(t), \;\; \rho_z = 0 \quad \text{on} \quad z = 1, \tag{2.5}$$

$$u_z = 0, \;\; w = w_0(x)r(t), \;\; \rho_z = 0 \quad \text{on} \quad z = 0, \tag{2.6}$$

$$u = 0, \;\; w_x = 0, \;\; \rho_x = 0 \quad \text{on} \quad x = 0, A^{-1}. \tag{2.7}$$

Slip boundary conditions are used on all boundaries to avoid the formation of sharp boundary layers that would need to be resolved by the numerical method. The main interest here is in the interior of the domain and near the sink. The initial conditions are

$$u = w = p = 0, \quad \rho = -\tanh(S(z - h_0)), \tag{2.8}$$

where the initial interface sharpness is determined by the sharpness parameter S and h_0 is the initial interface height. The flow out of the cavity is ramped smoothly from 0 at $t = 0$ via the ramping function

$$r(t) = 1 - \exp(-t/t_r), \tag{2.9}$$

where t_r is the ramping time. The drain velocity $w_0(x)$ is chosen to avoid sharp changes at the edge of the drain. Here

$$w_0(x) = \begin{cases} -\dfrac{1}{x_d}(1 + \cos(\pi x/x_d)), & 0 < x < x_d, \\ 0, & x_d < x < A^{-1}, \end{cases} \tag{2.10}$$

where x_d is the drain width.

While fluid is withdrawn exclusively from the lower layer, the interface drops with mean velocity $-Ar(t)$. The mean height of the interface under these conditions is

$$h_i(t) = h_0 - A(t - t_r(1 - \exp(-t/t_r))). \tag{2.11}$$

Another parameter of relevance is the effective Froude number based on the interface height. This is given by

$$Fr_i(t) = \frac{Q}{\sqrt{g' h_i^3}} = Fr_0 h_i^{-3/2}. \tag{2.12}$$

Note that since the interface drops down as time progresses, upper-layer fluid must eventually be drawn into the sink.

3. Linearized solution

In the case of flow of an ideal fluid, we can derive a set of linear equations that can be solved analytically to produce solutions that represent an approximation to the flow considered in this paper. This will provide a basis for comparison of the finite-difference solution with the idealized flows considered in some of the earlier papers. Taking the limit as $Re \to \infty$ in equations (2.1)–(2.4) and considering two distinct fluid layers, we end up with the irrotational flow of an inviscid incompressible fluid, and thus we can define velocity potentials $\phi_j, \;\; j = 1, 2$ for which

$$\nabla^2 \phi_j = 0, \;\; j = 1, 2. \tag{3.1}$$

Here ϕ_1 is the velocity potential in the lower layer, of density ρ_1, and ϕ_2 is that in the upper layer with density ρ_2. To maintain this model we must assume the interface between the layers is infinitesimally thin and that the fluids are immiscible.

The Navier–Stokes equations then reduce to the Bernoulli equation for the pressure, i.e.

$$\phi_{jt} + z_j + Fr_0^2(\phi_{jx}^2 + \phi_{jz}^2) = p_j, \quad j = 1, 2. \tag{3.2}$$

Our interest here is to ensure that there is no pressure jump across the interface and consequently these conditions in the two layers can be matched at the interface to give

$$\phi_{1t} - \gamma\phi_{2t} + \tfrac{1}{2}\left[\boldsymbol{q}_1^2 - \gamma\boldsymbol{q}_2^2\right] + 2Fr_0^{-2}(h_0 + \eta) = 2Fr_0^{-2}h_0, \tag{3.3}$$

where $z = h_0 + \eta(x, t)$ is the elevation of the interface, $\gamma = \rho_2/\rho_1$ is the density ratio, $\boldsymbol{q}_j$, $j = 1, 2$ is the velocity in the two layers, and Fr_0 is the bulk Froude number. In addition, there is a kinematic condition that the interface is a moving surface, and so we obtain

$$\eta_t + \phi_{1x}\eta_x - \phi_{1z} = 0, \tag{3.4}$$

$$\eta_t + \phi_{2x}\eta_x - \phi_{2z} = 0, \tag{3.5}$$

both on $z = h_0 + \eta(x, t)$. There are also initial conditions on the interface. First, we assume that the interface is flat

$$\eta(x, t = 0) = 0, \tag{3.6}$$

and that the velocity potential felt by the interface is that due to the initial background potential flow:

$$\phi(x, h_0, t = 0) = \phi_V(x, h_0), \tag{3.7}$$

where $\phi_V(x, z)$ is the potential flow solution for flow towards a sink in a vertical duct with uniform vertical flow at the top of the upper layer (see below). This initial condtion for ϕ is the natural choice given the formulation used for the numerical simulations. Buoyancy effects vanish in the limit as $t \to 0^+$.

Linearizing about the initial interface height and neglecting all quadratic terms, these equations on the interface reduce to

$$\phi_{1t} - \gamma\phi_{2t} + 2Fr_0^{-2}\eta = 0, \tag{3.8}$$

$$\eta_t - \phi_{1z} = 0, \tag{3.9}$$

$$\eta_t - \phi_{2z} = 0, \tag{3.10}$$

all on $z = h_0$. On the other boundaries (except at the sink) we have conditions that the fluid cannot flow through the walls and must be uniform at the upper surface, and so we obtain

$$\phi_{jx} = 0 \quad \text{on } x = 0, A^{-1}, \ j = 1, 2, \tag{3.11}$$

$$\phi_{1z} = 0 \quad \text{on } z = 0, \tag{3.12}$$

$$\phi_{2z} = A \quad \text{on } z = 1. \tag{3.13}$$

The solution in both layers is obtained as a perturbation about the potential flow of a fluid into a line sink in the bottom corner of a vertical duct with uniform vertical flow at the top of the upper layer ($z = 1$), i.e.

$$\phi_V(x, z) = -\frac{1}{\pi}\log\left(\cosh(A\pi z) - \cos(A\pi x)\right) + \sum_{k=0}^{\infty} f_k \cos\lambda_k x \cosh\lambda_k z, \tag{3.14}$$

where $\lambda_k = k\pi A$, $k = 1, 2, \ldots$ and f_k, $k = 1, 2, \ldots$ satisfy

$$\sum_{k=0}^{\infty} f_k \cosh\lambda_k \cos\lambda_k x = -A + A\left(\frac{\sinh A\pi}{\cosh A\pi - \cos A\pi x}\right) \quad \text{on } 0 < x < A^{-1}. \tag{3.15}$$

In other words, for each layer, we seek functions $\boldsymbol{\Phi}_j(x, z, t)$, $j = 1, 2$, such that

$$\phi_j(x, z, t) = \phi_V(x, z) + \boldsymbol{\Phi}_j(x, z, t), \quad j = 1, 2. \tag{3.16}$$

The $\boldsymbol{\Phi}_j$, $j = 1, 2$ are chosen as appropriate eigenfunction expansions that satisfy all conditions except those on the interface. Series coefficients are then found that satisfy these conditions and the initial condition. The correct form for $\boldsymbol{\Phi}_j$, $j = 1, 2$ can be shown to be

$$\boldsymbol{\Phi}_1(x, z, t) = a_0(t) + \sum_{k=0}^{\infty} a_k(t)\cosh(\lambda_k z)\cos(\lambda_k x), \tag{3.17}$$

$$\boldsymbol{\Phi}_2(x, z, t) = b_0(t) + \sum_{k=0}^{\infty} b_k(t)\cosh(\lambda_k(z-1))\cos(\lambda_k x), \tag{3.18}$$

where $\lambda_k = Ak\pi$, $k = 0, 1, 2, \ldots$. Now equating (3.9) and (3.10) and substituting these series, we find a relationship between the series coefficients,

$$a_k = b_k \frac{\sinh(\lambda_k h_0)}{\sinh(\lambda_k(h_0 - 1))} \quad (k = 1, 2, 3, \ldots), \tag{3.19}$$

and then substituting into the result of differentiating equation (3.8) and eliminating η_t using (3.9), and using (3.19) to eliminate b_k, gives a differential equation for each of the series coefficients a_k, i.e.

$$a_k''\left[1 - \gamma\left(\frac{\tanh(\lambda_k h_0)}{\tanh(\lambda_k(h_0 - 1))}\right)\right] + a_k\left(2Fr_0^{-2}\lambda_k \tanh(\lambda_k h_0)\right) = -Fr_0^{-2}\left(\frac{d_k}{\cosh(\lambda_k h_0)} + f_k\frac{\sinh\lambda_k h_0}{\sinh\lambda_k}\right), \tag{3.20}$$

where the d_k are the series coefficients obtained from the initial conditions on the flow,

$$\sum_{k=1}^{\infty} d_k(t)\cos\lambda_k x = A\left(1 - \frac{\sinh(A\pi h_0)}{\cosh(A\pi h_0) - \cos(A\pi x)}\right). \tag{3.21}$$

This is a second-order non-homogeneous differential equation for the series coefficients as functions of time, and can be solved using standard techniques to give

$$a_k(t) = A_k \cos\sqrt{\frac{\beta_k}{\alpha_k}}t + B_k \sin\sqrt{\frac{\beta_k}{\alpha_k}}t + 2Fr_0^{-2}\frac{1}{\beta_k}\left(\frac{d_k}{\cosh\lambda_k h_0 + f_k(\sinh\lambda_k h_0/\sinh\lambda_k)}\right) \quad (k = 1, 2, 3, \ldots), \tag{3.22}$$

where A_k and B_k are obtained by applying (3.6) and (3.7). Noting equation (3.9) and integrating the series for ϕ_{1z} with respect to t, we finally obtain

$$\eta(x, t) = h_0 - At - \sum_{k=1}^{\infty}\frac{d_k}{\omega_k}\cos\lambda_k x \sin\omega_k t, \tag{3.23}$$

where

$$\omega_k = \sqrt{\frac{\beta_k}{\alpha_k}}, \quad \beta_k = 2Fr_0^{-2}\lambda_k \tanh \lambda_k h_0, \tag{3.24}$$

and

$$\alpha_k = 1 - \left(\frac{\gamma \tanh \lambda_k h_0}{\tanh \lambda_k (h_0 - 1)} \right) \quad (k = 1, 2, 3, \ldots). \tag{3.25}$$

This solution not only allows us to compute the approximate shape of the interface at any time, but also enables us to make computations of the interfacial wave speed. This can be obtained by noting that the dominant term in the equation is the first mode wave, and that this wave will travel fastest along the channel. The first mode wave speed will be

$$c_1 = \omega_1/\lambda_1 = \frac{1}{Fr_0} \sqrt{\frac{\tanh(A\pi h_0)\tanh(A\pi(h_0 - 1))}{A\pi(\tanh(A\pi(h_0 - 1)) - \gamma \tanh(A\pi h_0))}}. \tag{3.26}$$

Note that this depends on the respective layer depths and the density difference between the two layers, and is inversely proportional to the Froude number. Note also that (3.23) includes a term that represents the vertical drop of the interface level, even though we are evaluating about the undisturbed level of the interface. Eventually, this drop will invalidate the solution.

4. Numerical method

The system of equations (2.1)–(2.4) are solved using the method described by Armfield (1991). The method is a SIMPLE-type scheme applied on a non-staggered mesh with Leonard's (1979) QUICK correction for advection terms. A detailed description of the SIMPLE scheme can be found in Patankar (1980). Here, the approximate pressure equation is formulated so that the scheme is elliptic (Armfield 1991). A number of simulations are reported here using a range of discretizations. For the typical case where $A^{-1} = 4$, a non-uniform grid of 164×102 points is used. The grid has a finer vertical and horizontal resolution around the sink to resolve the stronger gradients there. A time step of $\Delta t = 5 \times 10^{-6}$ is used in all simulations.

All simulations reported here assume the stratifying agent is salt, giving $\sigma = 381$. This means that there is very little diffusion of the stratifying agent for the duration of the simulations. The ramping parameter is set to $t_r = 0.07125$ for most simulations. This is generally shorter than the time scales of interest here.

5. Results and discussion

5.1. *Introductory remarks*

A considerable number of simulations have been carried out with a range of values for the physical parameters. However, most simulations exhibit similar features, the main variation is in their relative importance and the order in which they occur. Table 1 summarizes the input parameters for the simulations as well as some important outputs. In the following subsection, an example simulation (Run 15, see table 1) that shows all the flow features of interest is described in detail. This provides a framework for later discussion.

Run	A^{-1}	S	Fr_0	Re	h_0	$Fr_i(0)$	h_d	t_r	c_l	c_n	Fr_d
1	2.5	25	0.072	500	0.6	0.1549	0.1546	7.125×10^{-2}	6.42	6.12	1.1849
2	4	25	0.036	500	0.6	0.0775	0.1130	7.125×10^{-2}	13.29	13.69	0.9477
3	4	25	0.072	500	0.2	0.8050	0.1803	7.125×10^{-2}	5.47	–	0.9405
4	4	25	0.072	500	0.25	0.5760	0.2085	7.125×10^{-2}	5.90	–	0.7565
5	4	25	0.072	500	0.3	0.4382	0.2011	7.125×10^{-2}	6.23	7.10	0.7982
6	4	25	0.072	500	0.35	0.3477	0.1605	7.125×10^{-2}	6.48	6.46	1.1197
7	4	25	0.072	500	0.4	0.2846	0.1647	7.125×10^{-2}	6.64	6.07	1.0776
8	4	25	0.072	500	0.5	0.2036	0.2059	7.125×10^{-2}	6.77	6.97	0.7705
9	4	25	0.072	500	0.6	0.1549	0.1658	7.125×10^{-2}	6.64	6.7.13	1.0663
10	4	25	0.072	500	0.7	0.1229	0.1908	7.125×10^{-2}	6.23	6.91	0.8642
11	4	25	0.072	500	0.8	0.1006	0.1721	7.125×10^{-2}	5.47	6.34	1.0081
12	4	25	0.144	500	0.6	0.3098	0.2374	7.125×10^{-2}	3.32	3.23	1.2448
13	8	25	0.072	500	0.4	0.2846	0.1789	7.125×10^{-2}	6.76	6.10	0.9518
14	8	25	0.072	500	0.6	0.1549	0.1876	7.125×10^{-2}	6.76	7.74	0.8861
15	12	25	0.072	500	0.6	0.1549	0.1989	7.125×10^{-2}	6.79	7.55	0.8119
16	12	12.5	0.072	500	0.6	0.1549	0.2235	7.125×10^{-2}	6.79	6.99	0.6816
17	12	25	0.072	500	0.6	0.1549	–	1.1425×10^{-2}	6.79	–	–
18	12	25	0.072	500	0.6	0.1549	–	7.125×10^{-4}	6.79	–	–
19	12	50	0.072	500	0.6	0.1549	–	7.125×10^{-4}	6.79	–	–
20	12	25	0.072	2000	0.6	0.1549	–	7.125×10^{-4}	6.79	–	–

TABLE 1. Summary of input parameters and some outputs for simulations. All simulations used $\sigma = 381$ and drain width $x_d = 0.25$. The numerical interfacial wave speed c_n is calculated by tracking the steepest part of the interface across the width of the cavity. The linear wave speed c_l is calculated from (3.26). Some data is missing for c_n as either no wave was visible before drawdown (Runs 3 and 4) or the run time was too short to allow its calculation (Runs 17 to 20). Runs 17 to 20 were terminated before drawdown occurred, hence neither h_d or Fr_d are available.

5.2. *Example simulation*

The initial flow in the interior of the domain is potential. Since the vertical velocity at the interface (defined by the $\rho = 0$ contour) is greatest above the sink, the interface dips towards the sink. As the interface dips, buoyancy acts to decelerate the downward flow. In this example simulation, buoyancy eventually overcomes the flow toward the sink and the interface 'bounces'. This bounce is characterized by the interface height no longer being a monotonic function of x. It can be shown that the time at which the bounce occurs is proportional to $Fr_i(0)$ and the magnitude of the interface deflection at this time is proportional to $[Fr_i(0)]^{-1}$. For the present simulation, the interface bounce occurs at $t \approx 0.11$. This bounce of the interface also signals the emergence of an interfacial wavefront from $x = 0$ which travels to the right, away from the sink. Figure 2 shows two snapshots of the density and streamfunction contours at $t = 0.5$ and $t = 1.0$. These two plots show the propagation to the right of an interfacial wave. At $t = 0.5$ (figure 2*a*), the wavefront is at $x \approx 3$. The wavefront is characterized not only by the shape of the interface, but also by the slopes of the streamlines in the upper layer. To the left of the wave front, the horizontal flow in the upper layer is to the right, away from the sink. To the right of the wavefront, the horizontal flow is towards the sink. In the lower layer, the streamlines are nearly parallel to the left of the wavefront and relatively evenly spaced: there is almost a plug flow towards the sink. To the right of the wavefront, the lower layer flow is much weaker. This structure is similar to a hydraulic model of the propagation of a wave generated

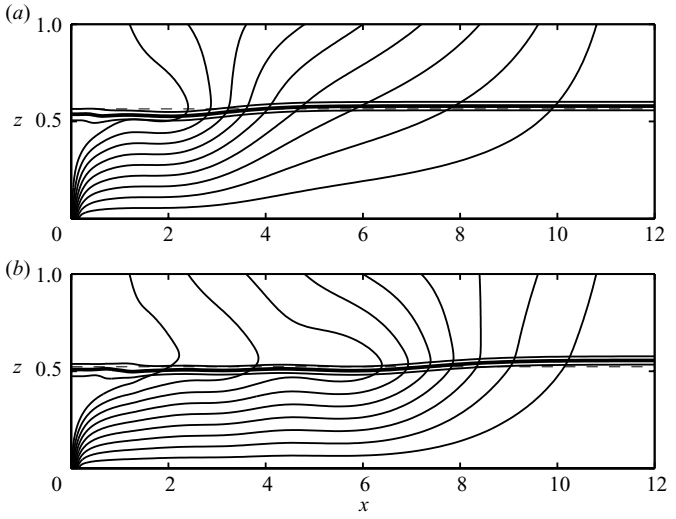

FIGURE 2. Density and streamfunction contours from Run 15 for (*a*) $t = 0.5$ and (*b*) $t = 1.0$. The heavy solid density contour is the zero contour corresponding to the interface. The solid contours are at $\rho = \pm 0.5$. The streamfunction contour interval is 0.1. The dashed line indicates the mean height.

near the sink: the lower layer is stagnant to the right of the wave front. By $t = 1.0$ (figure 2*b*) the wavefront has moved to $x \approx 8$. The propagation speed of the wavefront closely matches that predicted by linear theory. The overall structure is similar to that at $t = 0.5$: the horizontal flow in the upper layer changes sign at the wavefront and the flow ahead of the wavefront is nearly stagnant in the lower layer. There are some features here that are not captured by the linear or hydraulic results. Above the sink, there is some thickening of the interface which is consistent with the experimental observations mentioned earlier.

Figure 3 shows a number of snapshots of the interface for various times as the interfacial waves are generated and propagate away from the sink and then are reflected at the far endwall. Note that there is a natural vertical offset of these profiles as the average height of the interface drops as fluid is removed from the lower layer. By $t = 0.2$, the interface above the sink has already bounced and an interfacial wave is propagating to the right. As this wave propagates ($t = 0.2$ to $t = 1.2$) a train of smaller-amplitude waves are generated behind the main wavefront. The leading wavefront arrives at the endwall at $t \approx 1.2$, leading to a rapid downward movement of the interface there. This wave is then reflected and travels back towards $x = 0$. After this (and subsequent reflections), the interface has a complicated structure associated with the interference of left- and right-going waves. At $t \approx 2.4$, the initial wavefront has returned to $x = 0$, leading to a rapid downward movement of the interface above the sink. This pattern of waves travelling left and right continues until the height of the interface above the sink reaches some critical level where it is drawn into the sink (not shown in figure 3).

The above flow features are summarized in figure 4. This figure shows contours of density in the (t, z)-plane at either end of the domain. Also shown, for reference, is the mean height of the interface $h_i(t)$ given by (2.11). After the initial bounce (at $t \approx 0.11$), the interface at both ends of the domain drops at the same rate. Note that the drop rate is slower (by about 40%) than the drop rate of the mean height.

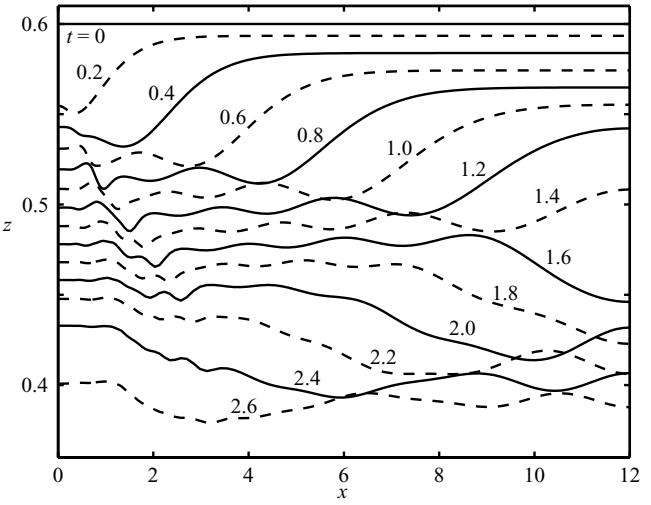

FIGURE 3. A sequence of interface profiles for various times from $t = 0$ to $t = 2.6$ from Run 15. Note that there is a natural vertical offset for these profiles as fluid is removed from the lower layer and the mean height of the interface drops.

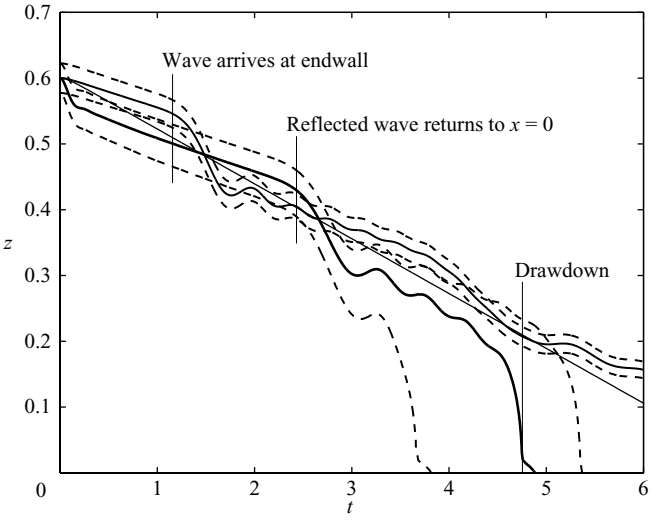

FIGURE 4. Contours of density in the (t, z)-plane at $x = 0$ and $x = 12$ from Run 15. The heavy solid contour is the zero contour and the dashed contours are at $\rho = \pm 0.5$. The thin solid line indicates the mean height $h_i(t)$ given by equation (2.11). The curve that intersects the t-axis at $t \approx 4.8$ is the interface height at $x = 0$.

Conservation of volume for the lower layer is ensured by the volume apparently removed from the lower layer by the propagating wavefront evident in figure 3. Also note that the interface thickens above the sink and thins at the endwall, consistent with experimental observations. At $t \approx 1.2$, the wavefront arrives at $x = 12$, leading to the large deflection of the interface there. Also evident in figure 4 is the train of smaller-amplitude waves trailing the main front. At $t \approx 2.4$, the reflected wavefront (and the associated trailing waves) arrive back at $x = 0$ leading to the large vertical deflection of the interface above the sink. There then follows a period of general

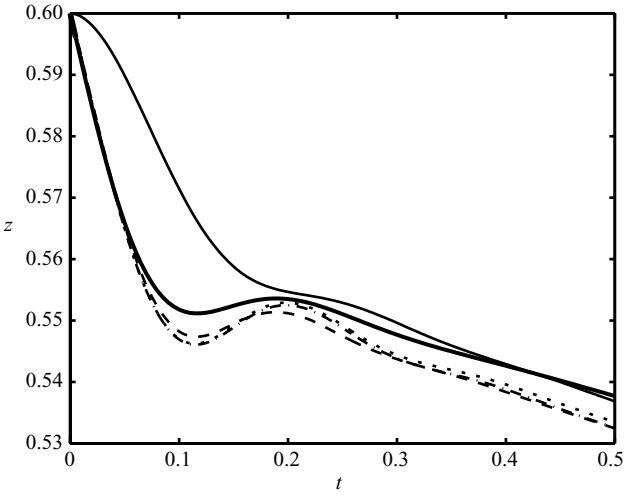

FIGURE 5. The interface height at $x = 0$ versus t from the linear results (heavy solid line) and selected numerical results: solid line Run 15, dot-dashed line Run 18, dashed line Run 19 and dotted line Run 20. Run 15 has a sink ramping time t_r 100 times longer than that of Runs 19 and 20 (see table 1 for further information).

waviness on the interface until, at $t \approx 4.7$, the height above the sink drops to a point where the interface is drawn rapidly into the sink.

5.3. *Comparison with linear solution*

Since much of the work on selective withdrawal from layered fluids has been performed using the assumptions of two layers of ideal fluid of different density separated by an infinitesimal interface, it is of great interest to compare the linearized solutions for such a model with the full simulations described in this paper. This process will serve the twofold purpose of validating the model, and, in turn, possibly validating the ideal-flow assumptions in the earlier work. Clearly, any linearized solution will not be able to show the highly nonlinear drawdown event, but it can be used to compare wave speeds, initial surface deflection, and to compare with simulations at different Reynolds numbers, outlet sizes, interface thicknesses and so on.

Figure 5 shows a comparison of the elevation of the middle of the interface above the outlet at $x = 0$. Several simulations are compared with the comparable linear solution. It is clear that changing the viscosity (increasing Re from 500 to 2000) has almost no effect on the behaviour of this point. Changing the interface thickness appears to reduce the amplitude of the bounce, and this is consistent with the linearized solution, which would have an interface of effectively zero thickness. The upper curve is an example of the solution for a more slowly ramped flow ($t_r = 0.07125$), and is given simply because most of the simulations were performed using this ramp function. The linear solution has an instant start, while the other cases are all started very rapidly, reaching almost full strength before $t \approx 0.01$. A separate linearized solution (not shown) reveals that the effect of a finite-sized hole is minimal as long as the hole is less than about $d = 0.8$, and even then it is still not particularly significant. All the numerical results predict a larger interface deflection than for the linear solution. This is for two reasons. First, the numerical results all have a finite-thickness interface. Secondly, nonlinear effects increase the initial deflection. As the interface is pulled

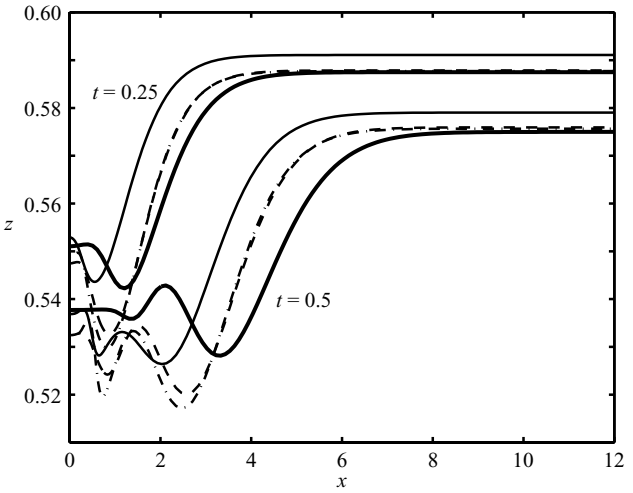

FIGURE 6. Interface profiles at $t = 0.25$ and $t = 0.5$ from the linear and numerical results corresponding to figure 5.

towards the sink, it feels the sink more strongly. However, for the linear solution, the sink strength felt by the interface is fixed to that at the starting height.

Figure 6 shows a comparison of the shape of the centre of the interface using the full simulation with the linearized interface solution at two different times. Although there is a slight offset in the location of the propogating wave, the wave speed and shape are accurately represented, again confirming that the simulation is realistic, and also that much useful information can be gained by using the idealized flow model. As noted above, the amplitude of the interfacial wave in the numerical solution is slightly greater than that for the linearized solution. The other noticeable difference is the degree of waviness behind the main wavefront. Making the interface thinner (Run 18 to Run 19 to the linear results) reduces this waviness. This can also be seen in figure 6 but is less obvious.

5.4. *The drawdown process*

A feature of past studies of withdrawal from a two-layer fluid is the examination of conditions for drawdown of the upper-layer fluid into the sink. It has been shown (Tyvand 1992; Landrini & Tyvand 2001; Stokes *et al.* 2003) that for the unsteady case, drawdown can occur at lower Froude numbers than predicted by steady-state solutions. The general picture of the drawdown process here is that as the interface drops, it eventually reaches a height above the sink when there is a sudden acceleration towards the sink and drawdown occurs (see figure 4). Figure 7 summarizes the drawdown Froude number Fr_d (i.e. Fr_i at drawdown) for $A^{-1} = 4$ for various starting heights and starting bulk Froude numbers Fr_0. There is substantial variation in Fr_d. For example, there is a significant jump in Fr_d from $h_0 = 0.3$ where $Fr_d = 0.80$ to $h_0 = 0.35$ where $Fr_d = 1.12$, a 40% jump. This strong dependence on h_0 reflects the effects of the waviness of the interface as the average height of the interface drops. As the interface drops, it supports a complicated wave pattern that causes the interface above the sink to oscillate about some mean height. As the mean height of the interface drops, these oscillations can cause the interface to drop locally to a level where buoyancy cannot overcome the acceleration towards the sink

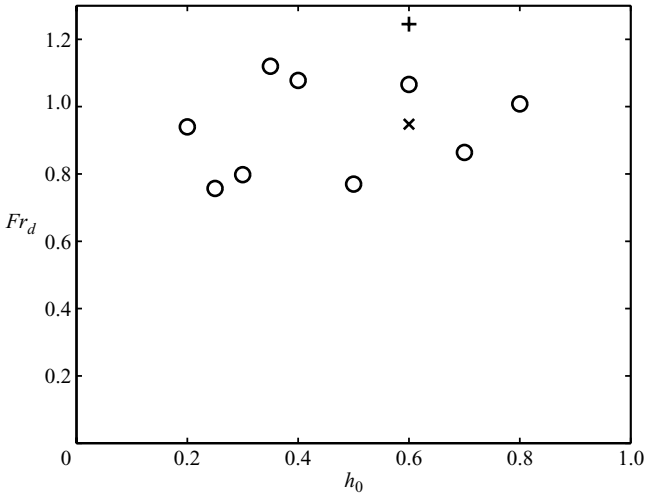

FIGURE 7. The drawdown Froude number Fr_d (based on the mean interface height $h_i(t)$ at drawdown) as a function of h_0 for $A^{-1}=4$. ○, $Fr_0=0.072$; +, $Fr_0=0.144$; ×, $Fr_0=0.036$.

and drawdown occurs. This process means that drawdown can occur over a range of Froude numbers – the precise timing of drawdown depends not only on h_0, but also wave amplitude, wave speed and the length of the domain. From figure 7, the range over which Fr_d varies decreases as h_0 increases (at least for fixed Fr_0). This is to be expected since as h_0 increases, the magnitude of the initial bounce of the interface (and thus the associated waves) decreases as h_0 increases. Also, there is some attenuation of the waves owing to viscosity which has a longer time to act for larger h_0. At $h_0=0.6$, Fr_d increases with increasing Fr_0, again reflecting the importance of wave magnitude in determining Fr_d.

The detailed processes that lead to the variability in Fr_d can be seen in figure 8 which shows interface profiles just prior to drawdown for a variety of starting heights h_0. For $h_0=0.2$ (figure 8*a*), the interface is rapidly drawn into the sink. In fact, this occurs before the effects of buoyancy on the interface are apparent. For $h_0=0.25$ (figure 8*b*), however, the interface bounces before it is drawn into the sink. Note that the bounce causes the interface height to have a local minimum away from $x=0$. This property persists and is exaggerated as the interface is drawn into the sink. This means that, for this finite-width sink case, upper-layer fluid is first drawn into the sink away from $x=0$ (where the sink velocity is greatest). A further effect of this bounce is that it slightly delays the drawdown of the interface leading to drawdown occurring at a lower Fr_d (see figure 5) than for $h_0=0.2$. For $h_0=0.3$, the effects of buoyancy on the interface are more pronounced with not only the bounce occurring, but also the correction of the overshoot – this is the process leading to the generation of the interfacial waves moving away from the sink, as discussed above. The effect of this additional recoil is that drawdown occurs at a higher Fr_d than for $h_0=0.25$. This effect is more pronounced for $h_0=0.35$ (figure 8*d*) where the initial bounce and correction has propagated away from the sink, leaving in its wake smaller oscillations above the sink (see figure 3). For the times shown in figure 8(*d*), the interface above the sink is falling more slowly than the mean rate as the wavefront generated by the initial flow propagates across the cavity – the interface profiles in figure 8(*d*) are more crowded than those in figure 8(*c*). This process delays drawdown leading

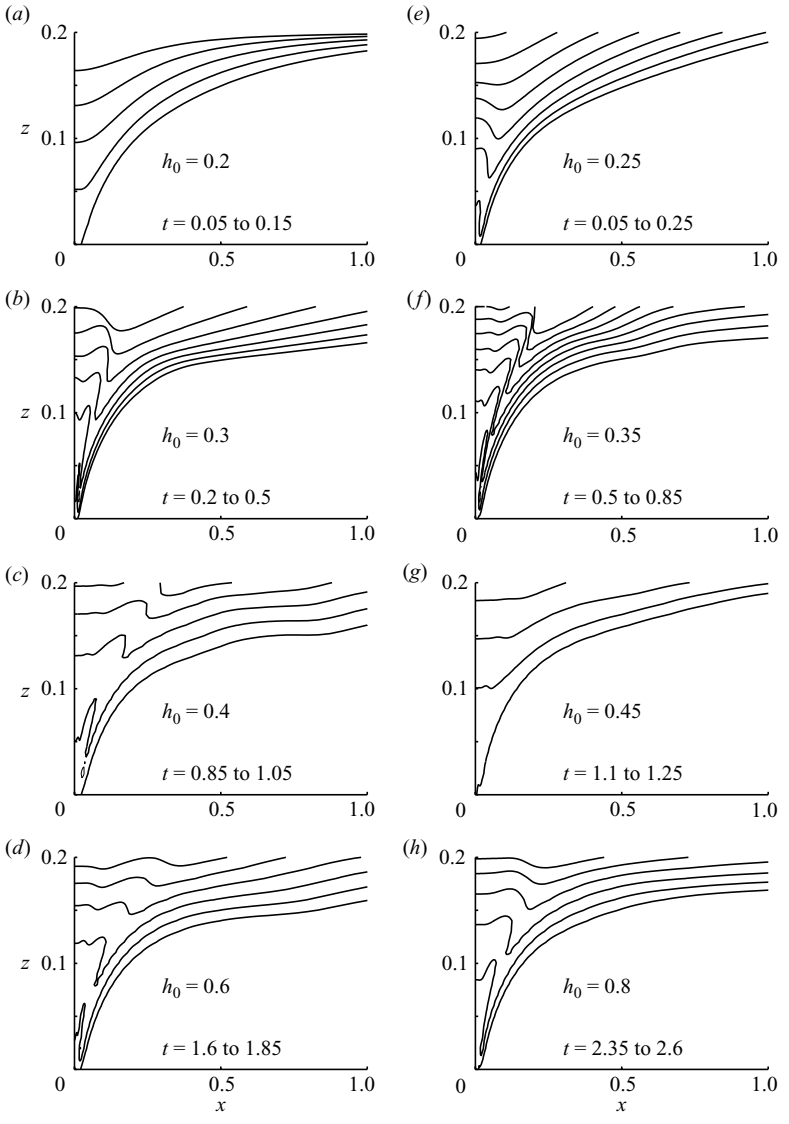

FIGURE 8. Sequences of interface profiles near the sink as drawdown occurs for various initial interface heights h_0 and $Fr_0 = 0.072$. The time between profiles is 0.025 for (*a*), (*b*) and (*f*) and 0.05 for (*c–e*) and (*g–h*). Note that in each case, drawdown occurs when the mean interface height has dropped to approximately 0.2.

to the significant jump in Fr_d from $h_0 = 0.3$ to $h_0 = 0.35$. For $h_0 = 0.4$ (figure 8*e*) a further effect of the waves becomes important. The wavefront generated shortly after $t = 0$ reaches the endwall at $x = 4$ at $t \approx 0.4$. The reflected wavefront returns to $x = 0$ at $t \approx 0.8$, around the time that the interface in figure 8(*e*) is nearing the critical height. The wave arriving at $x = 0$ has the effect of momentarily pushing the interface towards the sink, which in this case leads to a lower Fr_d than for $h_0 = 0.35$. The wave leads to a locally greater drop speed, as can be seen by the interfaces for figure 8(*e*) being more spread out than for figure 8(*d*). Although this effect of the reflected wave on the drawdown details is significant, Fr_d does not change all that

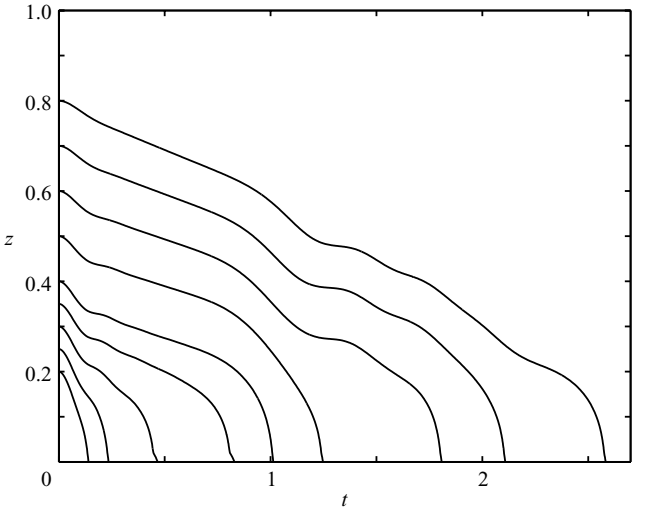

FIGURE 9. Interface height at $x = 0$ as a function of time for various starting heights h_0 from $t = 0$ until drawdown. For all simulations in this figure, $Fr_0 = 0.072$, $A^{-1} = 4$, $S = 25$ and $Re = 500$.

much from $h_0 = 0.35$ to $h_0 = 0.4$. This is because by the time the wave has returned to $x = 0$, the interface above the sink is already close to the critical height. The effect of the returning wave is more pronounced for $h_0 = 0.5$ (figure 8*f*) since the wave returns to $x = 0$ while the interface height is still well above the drawdown height. The downward velocity of the interface prior to drawdown for $h_0 = 0.5$ is about twice that for $h_0 = 0.4$. Drawdown at $h_0 = 0.5$ occurs at $Fr_d = 0.77$, significantly lower than $Fr_d = 1.08$ for $h_0 = 0.4$. For larger h_0 (figure 8*g*, *h*), the waviness of the interface is less significant in the drawdown process. For these cases, by the time the interface is close to the drawdown height, the peak to trough amplitude of the waves has been attenuated by dispersion and viscous damping. Also, the initial amplitude of the waves is lower for larger h_0.

The above effects on the flow leading to drawdown are summarized in figure 9 where interface height above the sink is plotted against time for various starting heights h_0. For $h_0 = 0.2$, the interface is drawn straight into the sink with buoyancy apparently not playing a significant role in the dynamics. For $h_0 = 0.25$, there is a slight bounce evident at $t \approx 0.2$, but drawdown occurs soon afterwards. The bounce is more pronounced for $h_0 = 0.3$, leading to an apparent delay in drawdown. This delay is more significant for $h_0 = 0.35$ with a noticeably reduced drop speed of the interface. The profiles for $h_0 = 0.35$ and $h_0 = 0.4$ look very similar except for the vertical offset. There is a difference just before drawdown as the reflected wave is just arriving at $x = 0$ for $h_0 = 0.4$. The reflected wave has a more significant impact for $h_0 = 0.5$, but for $h_0 = 0.6$ and greater, the downward deflection associated with the arrival of the reflected wave is insufficient to push the interface below its critical level. The interface for $h_0 \geqslant 0.6$ rebounds at $t \approx 1.2$.

6. Conclusions

In this paper, a series of simulations of the withdrawal of water from a tank of finite length containing a fluid with a two-layer stratification has been conducted. A

linearized ideal-fluid solution has also been computed and compared with the results of the simulations, both to verify the model and to examine the consequences of the approximations of the ideal-fluid model.

The simulations were conducted to investigate the critical drawdown flows, in particular, so that sensible comparisons can be made with earlier work and experimental results. It is clear that the major factor affecting drawdown in this situation is the finite length of the tank (when compared to the results from the idealized model). The transient wave activity due to the initiation of the sink flow causes a large degree of scatter in the results, in some cases delaying withdrawal and in others hastening it, depending on the phase of the waves reflected from the far end of the tank. The scatter can be reduced by increasing the depth of the lower layer so that the transient activity is smaller and has decayed more before drawdown occurs.

Comparison with the linear ideal model seems to indicate that the effects of Re and interface thickness are smaller than one might first think, and that the much simpler ideal models do produce meaningful results to this problem of stratified fluid withdrawal.

The results indicate that the critical drawdown Froude number (based on the lower-layer depth) is around $Fr_d \approx 1$, which in terms of the normal hydraulic Froude number would be around $\sqrt{2} \approx 1.42$. This compares very well with the critical drawdown Froude number computed in Hocking (1995) using the ideal two-layer steady-state model. Variability about this value can be explained almost completely by the wave activity.

For the purposes of numerical efficiency, the present results are computed with slip boundary conditions on all solid walls. In the laboratory, viscous boundary layers would form on these walls which would have some effect on the flow. Qualitively, this effect would correspond to the higher-density lower layer being apparently thinner as fluid within the boundary layer resists being moved. This would lead to a slight increase in flow speed in the lower layer, leading to a faster drawdown.

REFERENCES

Armfield, S. W. 1991 Finite-difference solution of the Navier–Stokes equations on staggered and non-staggered grids. *Comput. Fluids* **20**, 1–17.

Craya, A. 1949 Theoretical research on the flow of nonhomogeneous fluids. *La Houille Blanche* **4**, 44–55.

Gariel, P. 1949 Experimental research on the flow of nonhomogeneous fluids. *La Houille Blanche* **4**, 56–65.

Harleman, D. R. F. & Elder, R. E. 1965 Withdrawal from two-layer stratified flow. *J. Hyraul. Div. ASCE* **91**, 43–58.

Hocking, G. C. 1991 Withdrawal from two-layer fluid through a line sink. *J. Hydraul. Engng ASCE* **117**, 800–805.

Hocking, G. C. 1995 Supercritical withdrawal from a two-layer fluid through a line sink. *J. Fluid Mech.* **297**, 37–47.

Imberger, J. & Hamblin, P. F. 1982 Dynamics of lakes, reservoirs and cooling ponds. *Annu. Rev. Fluid Mech.* **14**, 153–187.

Jirka, G. H. 1979 Supercritical withdrawal from two-layered fluid systems. Part 1, two-dimensional skimmer wall. *J. Hydraul. Res.* **17**, 43–51.

Jirka, G. H. & Katavola, D. S. 1979 Supercritical withdrawal from two-layered fluid systems. Part 2, three dimensional flow into a round intake. *J. Hydraul. Res.* **17**, 53–62.

Kao, T. W. 1976 Selective withdrawal criteria of startified fluids. *J. Hyraul. Div. ASCE* **102**, 717–729.

Landrini, M. & Tyvand, P. A. 2001 Generation of water waves and bores by impulsive bottom flux. *J. Engng Maths* **39**, 131–170.

Lawrence, G. A. & Imberger, J. 1979 Selective withdrawal through a point sink in a continuously stratified fluid with a pycnocline. Tech. Rep. ED-79-002. Dept Civil Engng, University of Western Australia.

Leonard, B. P. 1979 A stable and accurate convective modelling procedure based on quadratic upstream interpolation. *Comput. Meth. Appl. Mech. Engng* **19**, 59–98.

Pao, H.-P. & Kao, T. W. 1974 Dynamics of establishment of selective withdrawal of a stratified fluid from a line sink. Part 1. theory. *J. Fluid Mech.* **65**, 657–688.

Patankar, S. V. 1980 *Numerical Heat Transfer and Fluid Flow*. Hemisphere.

Stokes, T. E., Hocking, G. C. & Forbes, L. K. 2003 Unsteady free surface flow induced by a line sink. *J. Engng Maths* **47**, 137–160.

Tyvand, P. A. 1992 Unsteady free-surface flow due to a line source. *Phys. Fluids* A **4**, 671–676.

Wood, I. R. & Lai, K. K. 1972 Selective withdrawal from a two-layered fluid. *J. Hydraul. Res.* **10**, 475–495.